

Landslides (2019) 16:893–906
 DOI 10.1007/s10346-019-01142-6
 Received: 30 September 2018
 Accepted: 31 January 2019
 Published online: 23 February 2019
 © Springer-Verlag GmbH Germany
 part of Springer Nature 2019

Ming Zhang · Lizhou Wu · Juncai Zhang · Liangping Li

The 2009 Jiweishan rock avalanche, Wulong, China: deposit characteristics and implications for its fragmentation

Abstract In this study, field investigation and numerical modeling using Particle Flow Code (PFC) were conducted to investigate deposit characteristics and their implications for the fragmentation mechanisms of the 2009 Jiweishan rock avalanche in Wulong, China. The results show that average grain-size distribution of the debris diminishes both from the proximal to the distal end and from the surface to the bottom of the deposit. A carapace of large boulders was formed at the surface and passively carried by the underlying finely fragmented debris during runout. Stratigraphic preservation, directly aligned boulders on the surface, and jigsaw fracture patterns exclude fragmentation mechanisms involving collision. Fragmentation induced by normal stress also cannot explain the progressive reduction in grain size of the deposit from the proximal to the distal end. Loose soil on the transport path was bulldozed to the very front and pushed passively by the rock debris, rather than remaining at the bottom and reducing frictional resistance between the debris and the ground. Thus, the undrained-loading hypothesis widely used to explain the long-runout of rock avalanches is not applicable. Shear-induced fragmentation is the most probable mechanism that can adequately explain the characteristics of the rock avalanche deposit.

Keywords Rock avalanche · Numerical modeling · Deposit characteristics · Fragmentation mechanisms

Introduction

Rock avalanches are notorious for their unexpectedly rapid long-runout, which can result in severe casualties and property destruction (Yin et al. 2009, 2017). The rock avalanche transport mechanisms have been studied for many decades but remain a challenging research topic in the international scientific community. In total, several tens of hypotheses have been proposed, with summaries in Davies (1982), Legros (2002), and Zhang et al. (2016). However, these hypotheses have been neither confirmed nor refuted, and how the granular debris is transported is still much debated today.

One important reason leading to the numerous transport hypotheses is that present researchers lack effective methods to obtain the dynamical parameters operating during transport. Transport of material in rock avalanches rarely is measured in the field due to their sudden failure, huge volume, and rapid movement beneath immense clouds of dust (Sosio et al. 2008; Imre et al. 2010; Li et al. 2012; Dufresne et al. 2016). Researchers usually have few opportunities to observe them in action or on film. Field investigations of rock avalanche deposits (Shreve 1968; Davies 1982; Strom 2004; Smith et al. 2006; McDougall et al. 2006; Zhang et al. 2011; Yin et al. 2011a, 2011b; Xing et al. 2014; Cox et al. 2015) have been hindered by both natural impediments such as lack of availability and accessibility of internal exposures and,

crucially, sampling method (Dunning 2006; Crosta et al. 2007). Physical modeling experiments (Savage and Hutter 1991; Hutter et al. 1995; Davies and McSaveney 1999; Davies et al. 1999; Okura et al. 2000; Friedmann et al. 2006; Manzella and Labiouse 2008; Imre et al. 2010; Richefu et al. 2012; Wang et al. 2016) are also not capable of modeling the high mobility of the rock avalanche due to the “size effect,” absence of significant fragmentation during motion owing to the low involvement of energy (De Blasio and Crosta 2014) and much fewer number of used grains or blocks (Friedmann et al. 2006). Empirical methods and statistical formulae (Scheidegger 1973; Davies 1982; Nicoletti and Sorriso-Valvo 1991; Legros 2002; Pedrazzini et al. 2012; Pudasaini and Miller 2013; Lucas et al. 2014) lack robustness, unless there is a comprehensive description of complex geological and geotechnical conditions (Tang et al. 2009).

Many researchers have tried to analyze the emplacement mechanisms through studying how grains are fragmented during runout, since pervasive fragmentation exists in rock avalanche debris and is considered closely related to the emplacement mechanisms. They have proposed four main fragmentation hypotheses, including fragmentation induced by collision (Deparis et al. 2008; Preuth et al. 2010; Cagnoli and Piersanti 2017), by shear (Davies and McSaveney 2009; McSaveney and Davies 2009; Zhang et al. 2016), by a combination of collision and shear (Crosta et al. 2007; Wang et al. 2015; Perinotto et al. 2015), and by high normal stress (Estep and Dufek 2013; De Blasio and Crosta 2014, 2015).

Deposits of rock avalanches can provide insights into fragmentation and transport mechanisms of rock avalanches. Through analyzing the distribution of rock avalanche deposits in the Mackenzie Mountains in Canada, Eisbacher (1979) hypothesized that streaming of the rock avalanche was initiated by momentum transfer from the back of a collapsing cliff through to its frontal disintegrating portion and facilitated by the dispersion of large blocks in finer interstitial material. Davies (1982), Dunning (2004), Campbell (2006), McSaveney and Davies (2009), De Blasio and Crosta (2014), Zhang et al. (2016), and Zhang and McSaveney (2017) suggested that rock avalanche debris formed a dense granular flow without free collisions, except within an about 10-m-thick surficial carapace, during runout. Crosta et al. (2007), through analyzing grain size data from the deposit of the 1987 Val Pola rock avalanche, proposed that more than a single comminution process acted during rock avalanche emplacement. Perinotto et al. (2015) demonstrated that dynamic disintegration continuously operated with increasing runout distance from the source, down to a grinding limit of 500 μm , by examining morphometric, grain size and exoscopic characteristics of various types of particles from volcanic debris avalanche deposits. Wang et al. (2015, 2016) proposed that both the overburden pressure and the self-excited vibration energized by an undulating ground

surface may play dominant roles in the particle dynamic fragmentation in the basal facies, based on morphological and statistical analyses of surface textures on quartz grains in the deposits of two earthquake-triggered rock avalanches. Dufresne et al. (2016), based on investigations of the Tschirgant deposit in Austria, stated that rock sliding and rock avalanche spreading occurred simultaneously and lithology had a very strong control on the final deposit morphology, with different lithologic units forming individual deposit surfaces. Dufresne and Dunning (2017) mapped rock avalanche facies in deposits at Tschirgant in Austria and at Flims in Switzerland, and proposed three main deposit facies—the carapace, the basal facies, and the body facies. The body facies could be divided into three sub-facies, including jigsaw-fractured facies and fragmented and shear zone band facies that can be linked to specific processes acting during rock avalanche emplacement.

However, these deposits are mostly larger than $1 \times 10^6 \text{ m}^3$ in volume and researchers have had few opportunities to observe their interiors (Zhang et al. 2016). Therefore, sections exposed by gullies incised by rainfall runoff and debris flow, and prospecting, including experimental drilling and excavation, have been used to examine the structure of the rock avalanche deposits (Crosta et al. 2007; Zhang and Yin 2013; Zhang et al. 2016). However, those approaches rarely allow a full examination of the internal structure of the whole deposit. Few rock avalanche deposits therefore have been fully investigated until now (Crosta et al. 2007).

Numerical simulation provides an alternative way to simulate the rock avalanche emplacement process, and consequently derive the structure of the deposits. The most commonly used methods are continuum methods and discrete element methods. Continuum methods are based on fluid mechanics (Munjiza 1999) and assume that the granular debris is a continuum material (Savage and Hutter 1989; Hungr 1995; Pirulli 2009; Sassa et al. 2010). They use the conservation equations of mass, momentum, and energy associated with different rheological models to describe the mechanical behavior of rock avalanches (Li et al. 2012). In addition, they adopt the proper constitutive law for the overall rock mass and the calibration of parameters (Forlati et al. 2001; Quecedo et al. 2004). Continuum methods are therefore at a disadvantage in simulating large-scale deformation and motion, especially those of rock avalanches, which are characterized by long travel distances, rock mass breakage, and granular debris movement. Discrete element methods are based on interaction (mechanical contact) laws (Munjiza 1999) and assume granular debris to be a discontinuous material, and they take into account the individual existence of each discrete grain forming the material (Staron and Hinch 2005; Aladejare and Wang 2017). The physical and mechanical properties of materials are defined through setting the parameters of the discrete elements composing the material and contacts between them. Discrete element methods obviously have an advantage if the modeling aims to simulate failure, fragmentation, and propagation processes and examine the internal structure of a rock avalanche deposit. Many authors have successfully reproduced propagation of granular debris of rock avalanche using discrete element methods (Okura et al. 2000; Pirulli et al. 2003; Taboada et al. 2005, 2006; Tang et al. 2009; Richefu et al. 2012; Li et al. 2012).

The catastrophic 5 June 2009 Jiweishan rock avalanche has been much studied for its precursors (Zhang and McSaveney 2018;

Zhang et al. 2018) and failure and initiation mechanisms (Xu et al. 2010; Yin et al. 2011b). However, its deposit and transport mechanisms, which are of great importance for hazard assessment (Chen et al. 2019; Wu et al. 2017, 2019), are rarely reported. Here, we used field investigation and discrete element modeling to study the deposit characteristics of the Jiweishan rock avalanche. Particular attention is given to the structure of the deposit, including the distributions of lithologies, the grain size and substrate (the original loose soil on the transport path), and their implications for the fragmentation mechanisms of the rock avalanche.

Case study

The Jiweishan rock avalanche occurred on 5 June 2009, and is located in Tiekuang Town, Wulong County, Chongqing, China (Fig. 1). The local geological authority had warned of the potential failure of the rock slope at least 10 years before, and some countermeasures, including evacuating more than 1000 people directly at the toe of the slope, had been taken. However, the authorities misjudged its failure mode, volume, movement direction and travel distance (Xu et al. 2010; Yin et al. 2011b), leading to 74 fatalities in an area that had not previously been considered to fall within the hazard zone (Zhang et al. 2018).

Methods

Remote sensing images taken by China Aero Geophysical Survey & Remote Sensing Center for Land and Resources on 6 June 2009 (the day after the rock avalanche) and a 1:10,000-scale map of the topography as it was prior to the event were used to analyze the general parameters and characteristics of the deposit.

Field investigation was conducted in October 2014, over 5 years after the event, to investigate the characteristics of the deposits by authors M. and J. Zhang. A portable GPS instrument was used to determine locations of the observation points on the remote sensing image and the topographic map.

Numerical modeling using the Particle Flow Code (PFC) software based on the discrete element method was conducted to study the internal structure of the deposit. Properties of the rock mass and the soil involved in the modeling were obtained from laboratory tests.

Geologic setting

The source area of the rock avalanche was on the edge of Jiweishan Mountain, which extends roughly in a north-south direction (Fig. 2). The cliff surface dips to the east and is a nearly vertical surface with a height of 50 to 150 m. Outcrops in the slope consist of four units of rocks; from the top down (Fig. 3):

- (1). Gray and white gray limestone of the Lower Permian Maokou Formation (P₁m), which is about 50 m in thickness. Karstification is strongly developed, with karst caves, fissures, and pipes widely distributed in this unit.
- (2). Dark gray limestone of the Lower Permian Qixia Formation is about 150 m in thickness and interbedded with thin layers of weaker shale about 10 to 30 cm thick. The sliding took place on the contact between the limestone and one of the shale layers. This formation has little internal karst development because the interbedded shale layers act as aquicludes, blocking rainfall seepage into the interior of the unit.

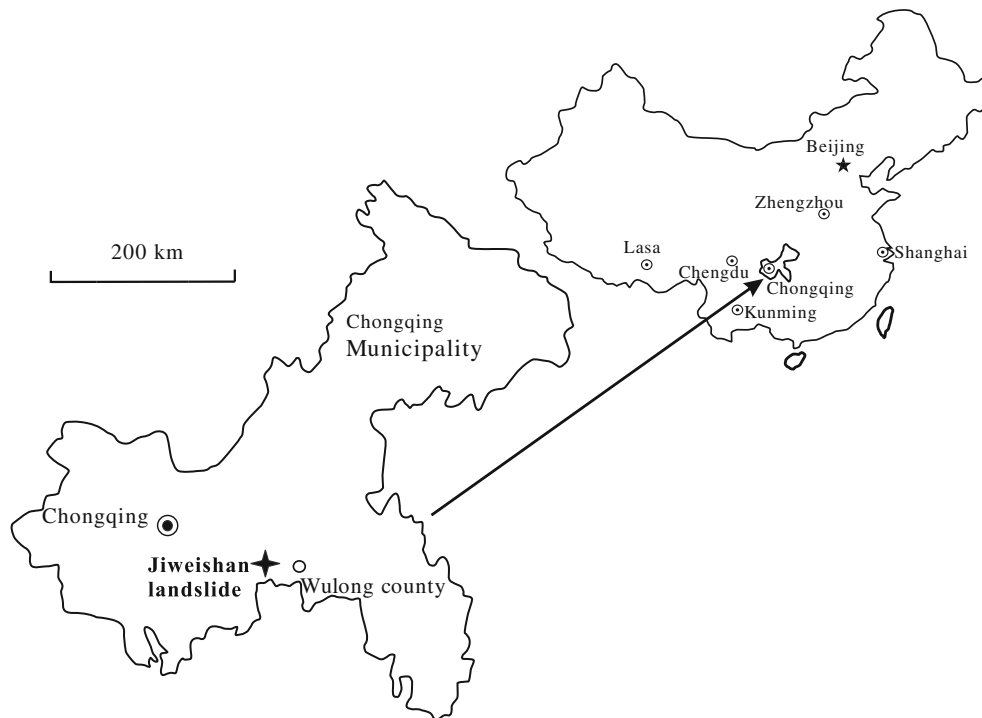


Fig. 1 Location of the Jiweishan rock avalanche

- (3). Claystone of Liangshan Formation of the lower Permian System (P₁l) is 10 to 14 m in thickness, with an iron ore layer less than 2.0 m thick in it.
- (4). Silt mud shale of Hanjiadian Formation is of the Middle Silurian System (S₂h).

A series of laboratory tests on the limestone of the Qixia Formation were conducted and its physical and mechanical properties were obtained, as presented in Table 1.

The above strata formed a monocline at the source area with a dip direction of 345° and a dip angle of 17 to 24°. The failed rock mass was incised by three sets of regional and vertical joints (Figs. 2 and 3). The first set is roughly parallel to the cliff surface with a strike in a roughly N-S direction. The second one is perpendicular to the cliff surface with a strike of roughly E-W. The third one intersects the cliff surface at about 35°. Two cracks, C₁ and C₂, a karstified zone developed along these three sets of joints, and the cliff surface defined the failed rock mass boundaries, and form its rear scar, west, front, and east boundaries, respectively (Fig. 2). Based on data from 3D laser scanner measurements, lengths of cracks C₁, C₂, karstification zone, and eastern boundary of the source area are 152 m, 480 m, 273 m, and 717 m, respectively (Yin et al. 201b). The thickness of failed rock mass varied between 50 and 80 m. The volume of the failed rock mass is about $500 \times 10^4 \text{ m}^3$. Before the rapid failure event, cracks C₁ and C₂ had opened and less than 40% of the area of the karstified zone remained intact (Yin et al. 201b). The rock mass suddenly failed due to the brittle failure of the bridges in the karstified zone (Zhang and McSaveney 2018).

In this study, we mainly focus on deposits of the Jiweishan rock avalanche and do not discuss its failure and initiation mechanisms, for which readers should refer to Xu et al. (2010), Yin et al. (201b), and Zhang and McSaveney (2018).

The Jiweishan rock avalanche deposit

The remote sensing image (Fig. 2) indicates that the length of the deposit is about 1500 m along the Tiejiang Creek, and the maximum width is 470 m. Its total area is about 483,000 m². By comparing the pre- and post-failure topographic maps, Yin et al. (201b) drew a map of topographic changes due to the rock avalanche, from which the longitudinal section map along the I-I ' section line in Fig. 2 was obtained. From the maps in the paper of Yin et al. (201b) and Fig. 2, elevations in the proximal area are now 0 to 50 m lower than those of the original ground surface because the original loose soil was entrained and transported away by the rock debris. The elevations in the other areas have increased due to the accumulated deposit accumulation. The exact thickness of the deposits cannot be calculated because the thicknesses of the total and the entrained loose soils are not available.

The deposit can be divided into four areas based on its lithological and particle-size distributions (Fig. 2).

- (1) The spray area on the east of the cliff surface. A thin layer of fine fragments with isolated large boulders is distributed in this area. The vegetation in and around this area was blown down and flattened due to the strong air blast (Yin et al. 201b).
- (2) The proximal area lies directly under the toe of the failure surface. Although this area decreased in elevation compared with the original ground surface, rock deposits in this area have formed a large hummock that is higher than the surrounding areas (Hewitt et al. 2008; Dufresne et al. 2016). The surface of the deposit in this area comprises big boulders, mainly with diameters ranging between 0.5 and 10 m (Fig. 4); the largest one reaches $30 \times 8 \times 15 \text{ m}$ in size. Most of these boulders were formed when the sliding rock mass broke apart along the two perpendicular original joints and the bedding

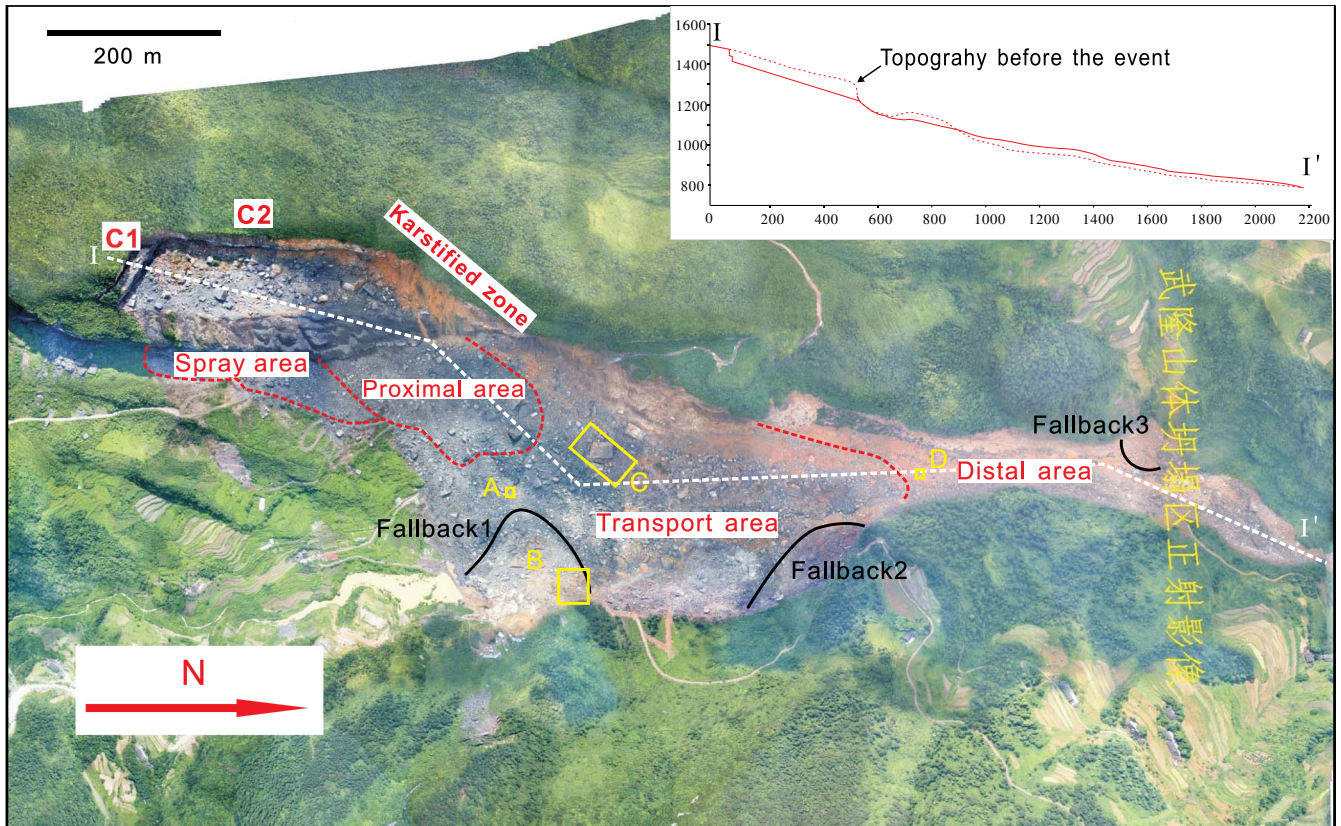


Fig. 2 Remote sensing image of the Jiweishan rock avalanche (taken by China Aero Geophysical Survey & Remote Sensing Center for Land and Resources on 6 June 2009). Yellow Chinese characters mean “Orthograph of Jiweishan rock avalanche.” White dashed line is longitudinal section I-I’ displayed in the top right corner. Red dashed lines are boundaries of different areas. Yellow rectangles are the locations of Figs. 4, 5, 6, and 7. Black lines are boundaries of fallbacks

planes of the rocks in the source area. The boulders are stacked together with large voids between them, and arranged in a disorderly way, with no directional arrangement. Much finer debris could be observed in the spaces between these big boulders. The visible debris in this area is mainly dark gray limestone of the Qixia Formation. There is no evidence that limestone of the Maokou Formation may underlie it.

- (3) Transport area in the middle part of the deposit. This area is between the proximal and the distal areas and has obvious streaming nature. Beside a small amount of dark gray limestone debris between the proximal area and an area where debris has fallen back (fallback 1 in Fig. 2, after Dufresne et al. 2016), most of the debris in this area is white gray and gray limestone of the Maokou Formation. Boulders at the surface are smaller than those in the proximal area, with diameters mainly less than 5 m; the largest one is a cuboid with $30 \times 22 \times 15$ m in size. Most of these boulders are distributed upon or among finer debris, rather than stacked with each other like the boulders in the proximal area.

Another conspicuous feature in the transport area is that most of the boulders at the surface are directionally arranged. Their long axes are roughly parallel to the transport direction of the debris (Fig. 5), indicating that the boulders in the surface were passively carried by the finer material below during movement; otherwise, their axes would be perpendicular to the transport direction, which is the orientation consuming the least amount of energy.

The granular debris ran up to the slope at fallback 1 (Fig. 2) and left a surge ridge, with a distinct thin layer of debris on the slope. Most of the debris collapsed back to the valley and formed a fan-shaped fallback deposit at the slope toe. A boulder of about $6 \times 8 \times 2$ m in size has run up to the slope shoulder, several meters higher than the crest of the surge ridge, with a little fine debris sporadically distributed between it and the debris margin. This further indicates that during movement, the big boulders at the surface were passively carried by the finer debris under them. When encountering obstacles such as the lateral mountains, the lower finer debris slowed down or stopped, while the upper large boulder was thrown up onto the slope shoulder due to inertia, with little frictional resistance (Fig. 6).

- (4) Distal area at the end of the transport path. This area has two prominent features. The first is that the debris is much finer—the particles are mainly less than 1 m in diameter. Several isolated large boulders on the surface were assumed to have rolled from uphill after the event. The rock debris is mainly limestone of the Maokou Formation. The second feature is that the content of the yellow loose soil entrained in the rock debris increases dramatically to be more than 50% in volume (Fig. 7), making the debris in this area look yellow in the remote sensing image (Fig. 2).

Based on field investigation and the remote sensing image, the general characteristics of the Jiweishan rock avalanche deposit can be summarized as follows:

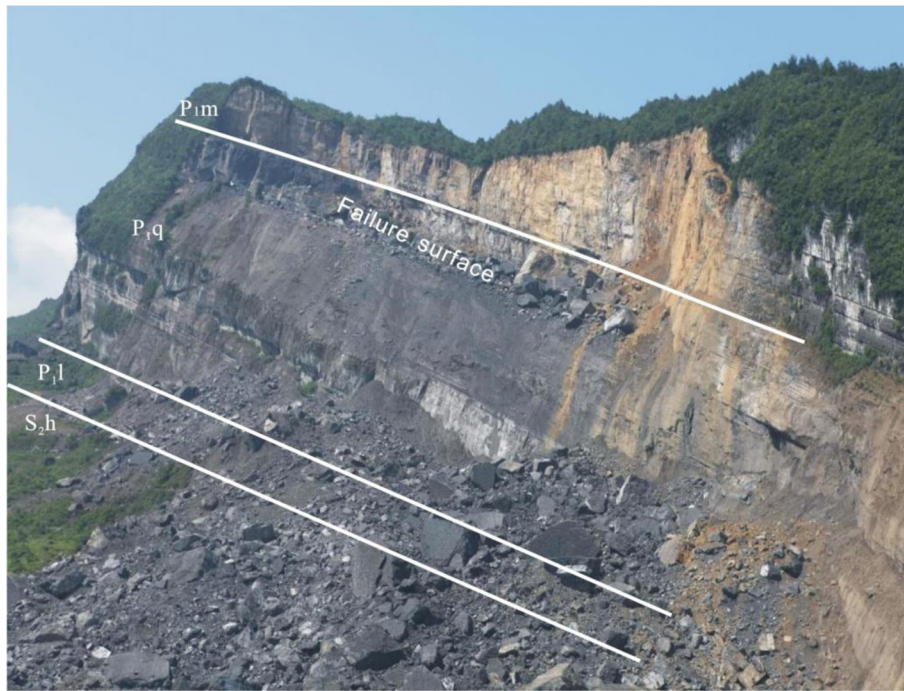


Fig. 3 Outcrops of the source area of the Jiweishan rock avalanche. P_{1m}—Lower Permian Makou Formation, P_{1q}—Lower Permian Qixia Formation, P_{1l}—Lower Permian Liangshang Formation, S_{2h}—Middle Silurian Hanjiadian Formation

- (1) The stratigraphic sequence in the source area is preserved in the deposit. The deposit is mainly composed of dark-gray limestone of Qixia Formation in the proximal area, mingled with a very small quantity of white gray limestone of the Maokou Formation. In the area between the proximal area and fallback 1, the lithology gradually changes from limestone of the Qixia Formation to limestone of the Maokou Formation. The debris at the surface changes from dark gray to white gray in color and karst depressions begin to appear in the boulders. The debris in the fallback area and the following zone in the transport area is mainly composed of white gray limestone of the Maokou Formation, mingled with a very small quantity of limestone of the Qixia Formation. In the distal area, rock fragments in the debris of soil and gravel mixtures are mainly limestone of the Moukou Formation.
- (2) A carapace consisting of big boulders remains at the surface of the deposit. In the proximal and the transport areas, the thickness of the carapace and diameter of the boulders in it gradually decrease with increasing travel distance. The boulders in the carapace are stacked together with each other above the finer debris in the proximal area, but are distributed on or among the finer debris in the transport area. The carapace tapers out in the distal area. The debris comprises yellow soil and finer fragments, which is indicated by thick vegetation on the surface 5 years after the event.
- (3) Substantial loose soil was entrained into the sliding debris and bulldozed to the distal end of the deposit. According to Yin et al. (2011b), at least a 50-m-thick layer of original valley floor sediment at some locations in the proximal area was entrained into the sliding debris, as well as the valley floor sediment along the transport path, and thus substantial sediment was assumed to be entrained into the debris. However, we cannot determine whether all the

sediment entrained was pushed to the front of the deposit, due to a lack of data on the original sediment along the path, and we were unable to calculate the volume of sediment in the front of the deposit.>

Numerical modeling

In order to model the internal structure of the deposit, we used a discrete element method, 2-dimensional PFC to simulate the initiation and the transport of the Jiweishan rock avalanche. This code has been successfully used to study transport mechanisms of granular material (Tang et al. 2009; Li et al. 2012). In this 2D code, basic elements are balls and walls of unit thickness. Balls are combined using different rules based on certain micro-parameters to form soils or rocks constituting the landslide, and walls are the boundaries of the model. The positions and contacts between balls and walls are updated iteratively from the contact forces, based on the laws of motion and force displacement (for the detailed principals and theories, readers should refer to Itasca (2004)).

Obviously, 2D modeling cannot simulate the 3D behaviors of a rock avalanche, including lateral spreading and collision with lateral mountains—both of these are very likely to diffuse the debris and reduce its kinetic energy, consequently reducing its travel speed and distance. In the Jiweishan rock avalanche, most of the debris was confined and traveled or deposited in Tiejiang Creek, except for a small part that ran up the lateral mountains and finally formed fallback deposits. To allow for kinetic energy loss due to friction and collision between the moving debris and lateral valley mountains, we can set the damping, which is used in the PFC to control the energy dissipation, to zero and adjust the numerical model until constraints such as the travel displacement and the deposit shape are consistent with the actual ones.

Table 1 Properties of the Qixia Formation limestone in the Jiweishan rock avalanche and micro-properties of balls composing the limestone in the numerical model

Properties of the Qixia limestone		Density	Young's modulus		Poisson's ratio	Unconfined compressive strength	Internal friction angle		Cohesion
Qixia limestone		2620 kg/m ³	K _n	K _s	0.229	256.9 MPa	Pb_nstr	Pb_sstr	41.72 MPa
Micro-properties for the Qixia limestone model		d	8.4 GPa	8.4 GPa	μ	Pb_K _n	40 MPa	40 MPa	λ
		2620 kg/m ³	8.4 GPa	8.4 GPa	0.5	Pb_K _s	40 MPa	40 MPa	1.0



Fig. 4 Big boulders are arranged in a disorderly way in the proximal area. The camera was facing southwest

Researchers (Staron 2008; Tang et al. 2009) indicate that the discrepancy between simulated results from 2D and 3D modeling is not significant and may be neglected, as long as the modeling is calibrated. Therefore, we believe we are justified in using the simpler 2D PFC to model the Jiweishan rock avalanche.

Numerical model

The numerical model that was built is based on the section map presented in Fig. 2. The slip surface, including the failure surface and the ground surface over which the rock mass transported was represented by walls, which were fixed as boundaries of the model. The sliding rock mass in the source area was composed of 1765 balls with uniformly distributed diameters between 1.6 and 2.4 m. To study entrainment of the loose colluvial soil, the colluvial soil, comprising 3144 balls with uniformly distributed diameters between 0.64 and 0.96 m, was set, based on the original topography and distribution of the colluvial soil. The number and size of the balls in this model were limited by the area which the balls filled and the power of the computer. A balance should



Fig. 5 Long axes of most of the boulders at the surface are directionally arranged in transport direction of the rock debris. The camera was facing roughly south



Fig. 6 Fallback 1, photographed from the opposite valley ridge. A big boulder of about $6 \times 8 \times 2$ m ran up to the top of the surge ridge. The camera was facing northeast

be reached between model resolution and practical simulation processing time (Li et al. 2012), which increases with an increasing number of balls. Also, to simplify the model and decrease the simulation process time, only three bedding planes and one set of 10 joints were modeled in the sliding mass. One of the bedding planes was the contact between limestones of the Maokou and the Qixia Formations; the other two were in the Maokou and Qixia Formations and separated them averagely, respectively. Ten joints were designed to represent the vertical joints in the original sliding rock mass and perpendicular to the bedding planes. To simulate brittle failure and rapid initiation of the sliding rock mass, a wall was set at its front toe, which was deleted immediately before the initiation.

The numerical model was displayed in two forms. Figure 8a displays the numerical model in a form of clusters. A cluster in PFC^{2D} is a group of balls bonded together to represent a rock or

soil particle and will be broken into smaller clusters or balls if stress exceeds its strength. In this study, they were designed to study fragmentation and grain size distribution of the deposits, and different clusters were displayed with different colors. Figure 8b is the model of the original sliding rock mass. Limestones of the Maokou and Qixia Formations were displayed in blue and green respectively. Figure 8c is the model of the loose soil on the transport path and is displayed in yellow. Both of them were designed to study distribution of the debris from different original parts in the final deposits.

Micro-properties adopted

It is important to set micro-properties of balls in the numerical model to simulate real rock and soil. Balls in a PFC model can be bonded to one another by using either contact bonds, parallel bonds, or both types of bonds (Itasca 2004). The sliding rock mass and colluvial soil were assigned different bond types and micro-properties based on their properties. The sliding rock mass was uniformly assigned the properties of limestone of the Qixia Formation for simplicity, and balls composing it were connected with parallel bonds, while those composing the colluvial soil were connected with contact bonds.

A parallel bond approximates the physical behavior of a cement-like substance lying between and joining the two bonded particles (Itasca 2004). Besides density, eight micro-parameters are required to characterize a parallel-bonded material, including normal and shear stiffnesses of the balls (K_n and K_s), normal and shear stiffnesses of the parallel bond (Pb_K_n and Pb_K_s), normal and shear strengths of the parallel bond (Pb_sstr and Pb_nstr), a particle friction coefficient (μ) and the radius ratio of the parallel bond (λ). In PFC, a numerical biaxial test is used to determine the micro-parameters of the balls through a trial-and-error process (Itasca 2004). A series of biaxial tests on granular samples with different micro-parameters were conducted in this study until the obtained macro-properties matched the mechanical properties of the Qixia limestone.



Fig. 7 Deposit at point D in Fig. 2, over 5 years after the event. The hammer (near the top) is about 30 cm in length. Yellow loose soil makes up over 50% of the debris in volume, which facilitates the growth of vegetation

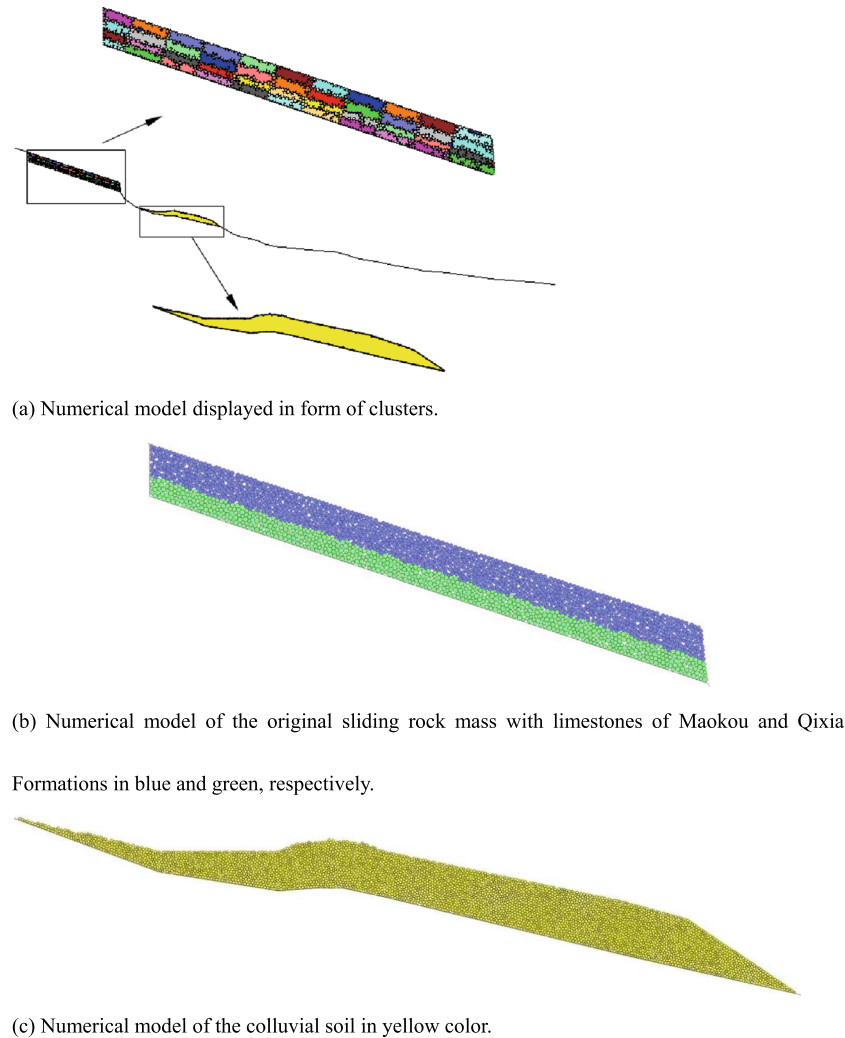


Fig. 8 Numerical model of Jiweishan rock avalanche was displayed in two different forms. Panel a is the numerical model displayed in clusters, which were designed to study fragmentation and grain size distribution of the deposits. Panels b and c are models of the original sliding rock mass and the colluvial soil, respectively, with different parts in different colors. Both were designed to study distribution of the debris from different original sources in the final deposits. Fifteen monitoring points were set in the model

The parameters including μ , λ , Pb_sstr , and Pb_nstr could be obtained directly from the numerical biaxial tests, while K_n and K_s , Pb_k_n and Pb_k_s should be calculated using the following equations:

$$K_n = K_s = 2E_c t \quad (1)$$

$$Pb_K_n = Pb_K_s = \frac{\bar{E}_c}{L} \quad (2)$$

where E_c is the Young's modulus at each particle-particle contact, and \bar{E}_c is the Young's modulus of each parallel bond. Both of them could also be obtained through the numerical biaxial tests.

The model granular sample used to conduct the biaxial test is shown in Fig. 9. It is 240 m in height and 120 m in width, and consists of 1232 balls. The particle-size distribution is the same as

that of the limestone in the numerical model of the Jiweishan rock avalanche presented in Fig. 8.

A series of tests with different micro-properties were conducted until the obtained macro-properties were similar to the properties of the Qixia limestone (see Table 1). When the micro-parameters of the balls and bonds equal the values presented in Table 1, the Young's modulus is 65.32 GPa, the unconfined compressive strength is 257.2 MPa, and Poisson's ratio is 0.231 (Fig. 9b).

Parameters of the balls on the surface of the joints and bedding planes, including Pb_sstr , Pb_nstr , and Pb_k_s , are set at half of those of the intact limestone, while μ , λ , K_n , K_s , and Pb_k_n are same as those of the intact limestone.

For the colluvial soil in the valley, we assigned six parameters. The density of the balls (B_d) is 1500 kg/m³, the normal and shear stiffnesses of the balls (B_K_n and B_K_s) are 10 MPa and 10 MPa, the normal and shear strengths of the contact bond (B_nstr and B_sstr) are 0.4 MPa and 0.4 MPa, and particle friction coefficient of the balls (B_mu) is 0.4 (Table 1), based on the numerical biaxial tests on the loose soil of the Jiweishan rock avalanche conducted by Zhang (2015).

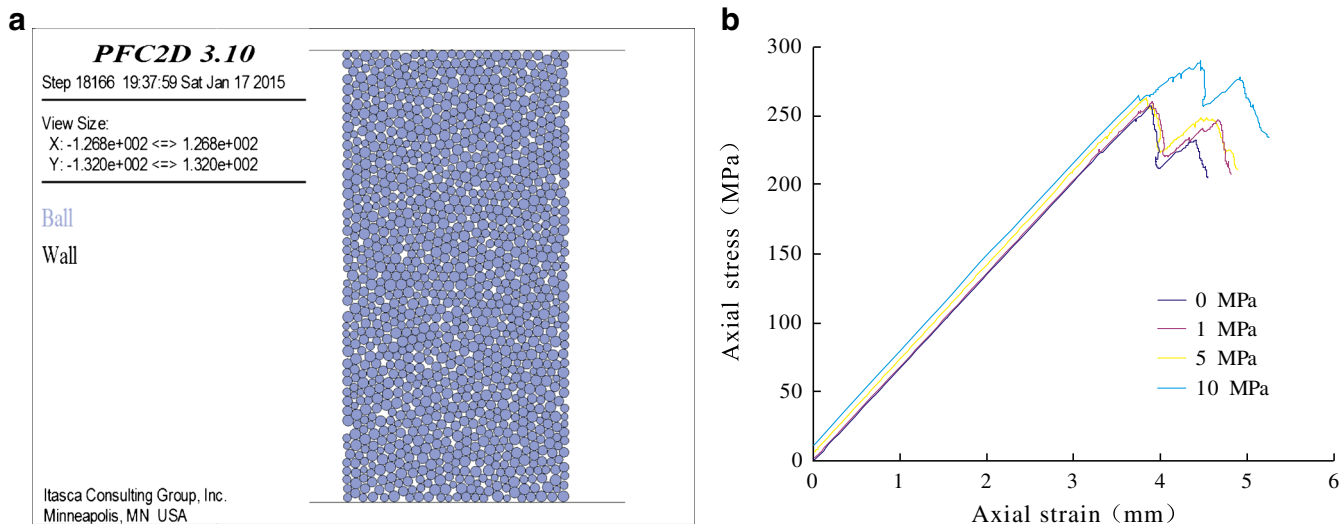


Fig. 9 Numerical biaxial tests. **a** Granular sample. **b** Stress-strain relationships from unconfined and confined compressive tests

For the wall, we set its normal and shear stiffnesses to 1×10^{10} Pa, which is large enough in case the balls sliding on it penetrate through it. Its friction coefficient, which is also the friction coefficient of the slip surface for the sliding rock mass and key for displacement of the rock avalanche, is used to calibrate the numerical model.

Numerical damping

Damping in PFC is a parameter used to control the energy dissipation by determining the coefficient of restitution of energy for individual grain-to-grain interaction during ball collision, and it could therefore accelerate the convergence of the numerical solution and control the landslide displacement. However, it is not a parameter that is explicitly related to any physical mechanisms (Tang et al. 2009). Therefore, it could not be obtained on the basis of any mechanical mechanisms, but only through back-analysis. Since the damping and friction coefficient of the wall are both parameters controlling the displacement of the landslide, we set the former to a constant and use the latter to calibrate the numerical model until displacement and deposit shape of the rock avalanche matched the actual one. We set damping to be 0, which implies that granular debris is a gravity-driven flow, and the drag force on the particles caused by air is negligible (Li et al. 2012).

Calibration of the numerical model

The numerical model must be calibrated using constraints such as displacement, movement speeds, and final deposit distribution, in order for the obtained modeling results to approach the real ones. In this simulation, particular attention was paid to the relationship between the rock avalanche displacement and the friction coefficient of the bottom wall, which is the slip surface of the sliding rock mass.

In the Jiweishan rock avalanche, the sliding rock mass moved the loose soil or on the shale of the Hanjiadian Formation at the valley bottom if the loose soil was scraped off. Under such circumstances, friction coefficients of less than 0.6, which is the empirical value of the friction coefficient of rock, were used to calibrate the numerical output until it matched the real displacement. Five coefficients, 0.6, 0.3, 0.25, 0.20, 0.15, and 0.1, were assigned to the slip surface, respectively, to reproduce the emplacement of the Jiweishan rock avalanche. It should be noted that sporadic balls ran away from the main debris, splashing

upwards or going ahead. They were set to be deleted automatically during the modeling.

Figure 10 shows the modeling results using different friction coefficients of the slip surface. When the friction coefficient is greater than or equal to 0.30, the travel distance of the rock avalanche is obviously less than the actual one. When the friction coefficient equals 0.2, although the travel distance is equal to the actual one, the obtained elevation in the proximal area is obviously higher than that before the event, and the final deposit is distributed mainly at the proximal part. When the friction coefficient is equal to 0.10, the travel distance is larger than the actual one and most of the deposit is at the distal part of the deposit. Outputs of the model with a friction coefficient of 0.15 are closest to the actual travel displacement and deposit distribution of the Jiweishan rock avalanche. Therefore, we used 0.15 as the friction coefficient of the bottom wall in this simulation.

It is worth noting that the degree of fragmentation of the deposit in the numerical model with the friction coefficient of 0.15 is also coincidentally closest to the real deposit. Tang et al. (2009) used fragmentation degree of the deposit as a constraint on the shear and normal strengths of the parallel bond to calibrate the numerical model. However, the fragmentation degree of the final deposit in a real rock avalanche cannot be exactly calculated at present due to its huge volume. Moreover, not only the bond strength but also the friction of the slip surface (see Fig. 10) influences the fragmentation degree of the sliding rock mass. Figure 10 indicates that the sliding rock mass with the friction coefficient of 0.15 has been disrupted significantly and most of the parallel bonds have been broken. Furthermore, the particle-size distribution of the model deposit is well in accordance with the actual deposit (more details will be described in the “Particle-size distribution in the deposit” section). Therefore, the fragmentation degree obtained for the numerical model, with a friction coefficient of the bottom wall of 0.15 and the bond strengths shown in Table 1, is deemed to be reasonable.

Results

Particle-size distribution in the deposit

Figure 11 presents the modeled deposit of the Jiweishan rock avalanche in the form of clusters. The single balls in navy blue

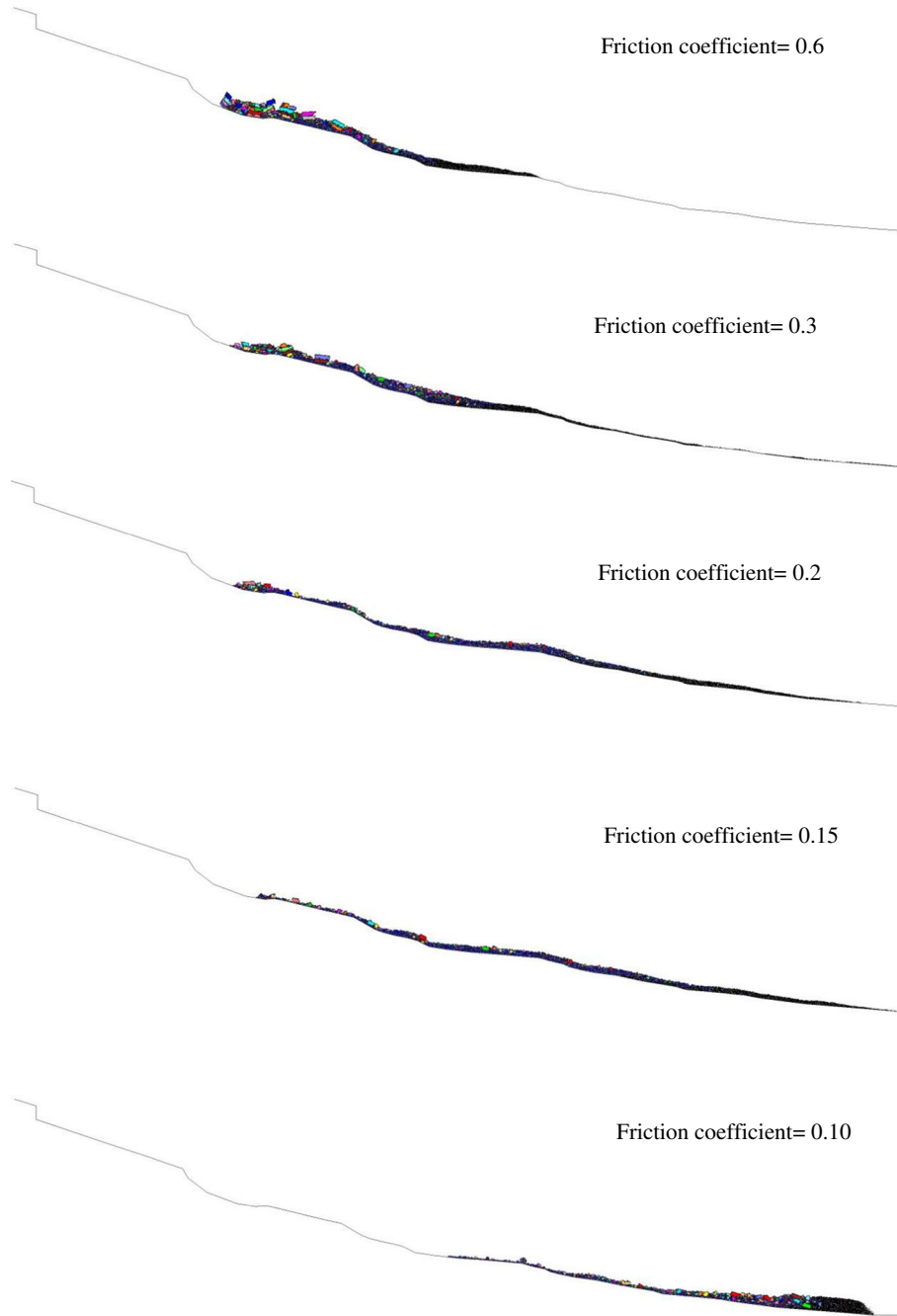


Fig. 10 Output of the numerical model with different friction coefficients for the slip surface of the Jiweishan rock avalanche

represent fragmented finer debris, while the clusters composed of more than one ball represent large boulders. Most of the boulders are distributed at the surface as a carapace on the back and middle parts of the deposits. A big-boulder area occurs near the proximal part of the deposits, where large boulders gathered. The pink boulder in this area is the largest one and obviously formed through breaking along the joints in the original sliding rock mass. From the proximal to the distal ends, the number and size of the boulders decreased with increased travel distance. At the distal part, single balls representing fine debris dominated, with only a few clusters mixed among them. Under the carapace at the surface,

the deposit is largely the fine debris, which is thinnest at the proximal end and thickest at the distal end. This means that the sliding rock mass experienced consecutive fragmentation during its emplacement. The distribution of modeled deposits accords well with what we observed in the field, and that observed in other rock avalanches (Zhang et al. 2016; Crosta et al. 2007; Perinotto et al. 2015).

Average grain size is also reduced from the surface to the bottom of the deposits. Large boulders are on the surface, and except at a very few locations, most areas of the bottom are covered by single balls representing the finest and thoroughly

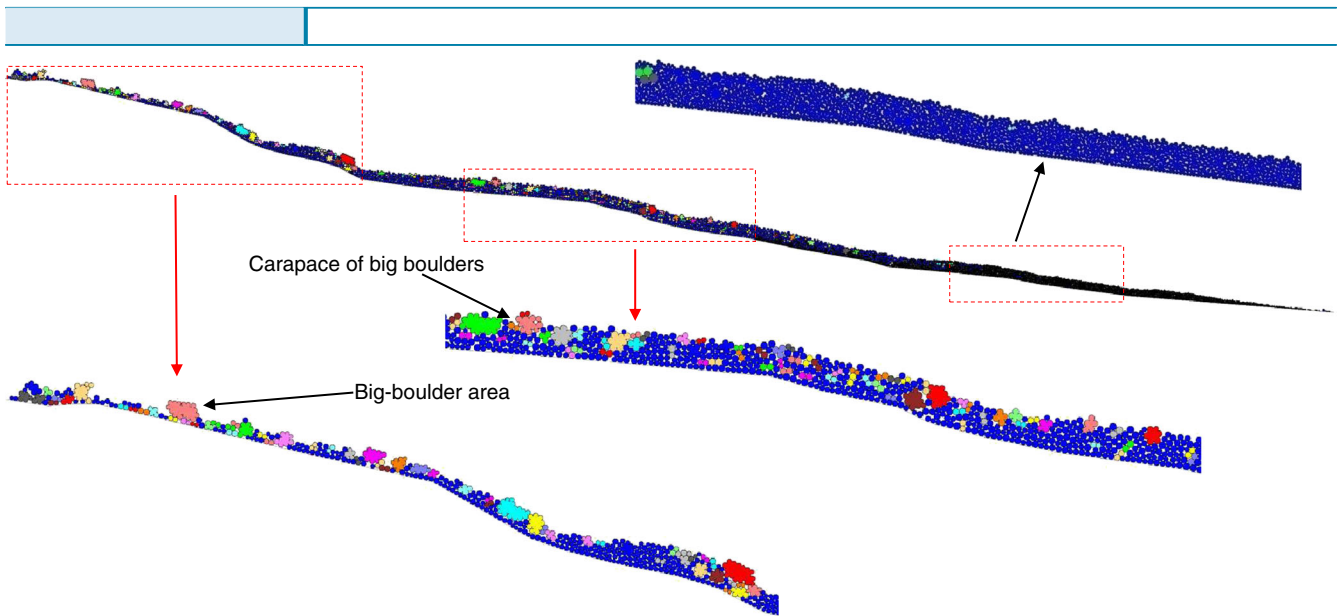


Fig. 11 Deposits of Jiweishan rock avalanche displayed in the form of clusters. There is a carapace of boulders at the surface and a big-boulder area at the proximal end at the slope toe

fragmented materials. Between the surface and the bottom are not thoroughly fragmented grains. But the transition between them in a certain section is not a gradual change such as the “inverse grading” seen in other rock avalanches (Crosta et al. 2007; Wang et al. 2015; Zhang et al. 2016), which may be due to the fact that number of balls of the numerical model and along a given section is not adequate to model this tendency.

Composition distribution in the deposit

Figure 12 shows deposits of the Jiweishan rock avalanche with limestones of Maokou and Qixia Formations and colluvial soil displayed in blue, green, and yellow, respectively, the same as in the numerical model in Figs. 8b and c. The blue balls representing limestone of the Maokou Formation are mainly distributed at the middle and upper part, while the green balls representing limestone of Qixia Formation are distributed at the back and lower part of the deposits. There is no obvious boundary between them. Some of the boulders of the Maokou Formation are scattered in those of the Qixia Formation, also some fine debris of the Qixia Formation are mixed with those of the Maokou Formation.

The yellow balls representing the loose soil originally on the transport path are distributed at the front part of the deposit, with sporadic blue and green balls mixed in them. Due to the push of rock debris behind, some hillocks have formed in the front part of the deposit. The boundary between the loose soil and the rock

debris is much clearer. It is interesting to note that almost all of the yellow balls were entrained and bulldozed to the forefront part of the deposits due to the huge kinetic energy evolved in the transport, rather than evenly distributed through the bottom of the deposits. This indicates that the yellow loose soil at the distal part we observed in the field and remote sensing image (Fig. 2) was almost the total amount of the loose soil originally lying on the ground surface where the rock debris was transported.

Discussions

Although there are some mixtures that include all three kinds of lithologies, deposits of the Jiweishan rock avalanche roughly maintain the stratigraphic sequence of the sliding rock mass in the source area, similar to other rock avalanches (Hewitt et al. 2008; Weidinger et al. 2014). In the Jiweishan rock avalanche, the emplacement process of the sliding rock mass could be deduced as follows. Because the rock mass reached its initial speed when sliding at the failure surface (Yin et al. 2011b; Zhang and Yin 2013), it forcefully collided with the ground at the cliff toe at an acute angle. The part of the limestone rock masses of the Qixia Formation directly contacting the ground during collision was stopped by the ground and deposited at the cliff toe. Most of the deposited rock masses that halted were formed through cracking along the three joints in the source area. They are therefore large boulders and formed an area of large boulders at the proximal

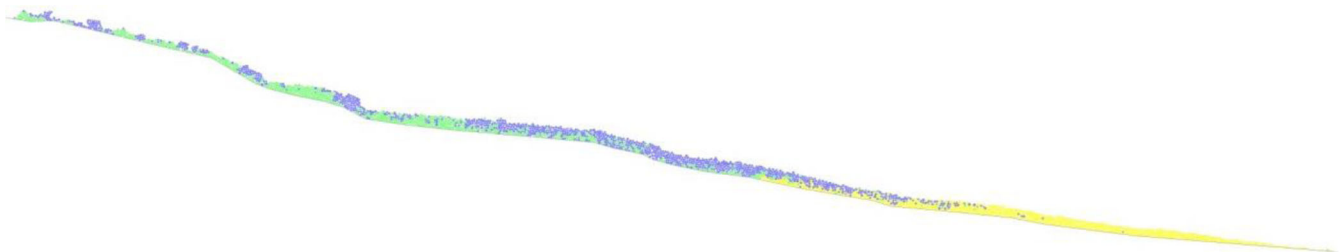


Fig. 12 Deposits of the Jiweishan rock avalanche displaying the distribution of limestones of the Maokou and the Qixia Formations and the loose soil (shown in blue, green, and yellow, respectively)

end. The Maokou limestone rock masses and the rest of the Qixia limestone kept moving after the collision. The uppermost Maokou limestone rock masses went to the forefront and then scraped the loose soil on the transport path. The rest of the Qixia rock masses followed and was deposited behind them. Therefore, the sequence of the sliding rock masses is preserved in the deposit.

At the surface of the Jiweishan rock avalanche deposit is a carapace with large boulders (Dunning 2004; Cagnoli and Manga 2004; Cagnoli and Romano 2013; Prager 2010; Davies and McSaveney 2012), underlain by much finely fragmented debris. The numerical modeling results indicate that the grain size decreased from the surface to the bottom, although the transition is not a gradual change, due to the limitation of our modeling. Results of the field investigation and numerical modeling both indicate that average grain size of the entire deposit consecutively decreased from the proximal to the distal ends. Although the deposit of the Jiweishan rock avalanche cannot be fully observed, our numerical modeling results accord well with the particle-size distribution of deposits of other rock avalanches (Crosta et al. 2007; Perinotto et al. 2015; Zhang et al. 2016). This indicates our modeling is credible.

The directionally aligned large boulders in the proximal area indicate that the carapace at the surface may have been carried by the underlying finer debris during runout and moved passively. Otherwise, the long axes of the boulders would be perpendicular rather than parallel to the transport direction. The large boulder running up to the lateral slope shoulder further indicates that the boulders were passively carried by the finer debris and ran up to the slope due to inertia when the finer debris was stopped by the lateral valley sides. Tang et al. (2009) reached a similar conclusion that the boulders at the surface did not roll and overturn and were not buried during motion in the Tsaoling rock avalanche triggered by the 1999 Chi-Chi earthquake, Taiwan, in that the inhabitants on the sliding rock mass survived during emplacement.

Stratigraphic preservation and directionally aligned boulders in the Jiweishan rock avalanche deposits and the jigsaw structure (Davies 1982; Davies and McSaveney 2009) widely found in deposits of rock avalanches all indicate that the finer debris under the carapace was moving as a dense granular flow during motion, in which grains maintain contact with surrounding grains. This view has been agreed by more and more scholars (Campbell 2006; McSaveney and Davies 2009; Dufresne et al. 2016; De Blasio 2011; Cagnoli and Romano 2013; De Blasio and Crosta 2014, 2015; Zhang and McSaveney 2017) in recent years. Therefore, the hypotheses suggesting fragmentation mechanisms in which collision is involved could be excluded. As for fragmentation induced by high normal stress, Zhang and McSaveney (2017) proved that rock debris under the normal stress of 600 kPa without shear showed little size reduction. This suggests that no size reduction would occur in the surface layer of at least 30-m thickness of the granular mass if only normal stress was applied. This violates the fact that the thickness of carapace of the deposit is less than 10 m, which is observed by Dunning (2004), Zhang et al. (2016), Davies and McSaveney (2012), and many others. De Blasio and Crosta (2014, 2015) proposed that grains are fragmented only on the steep slopes with angles greater than 70° above flat terrain due to the high normal stress induced by collision of the rock mass with the flat ground. But in the Jiweishan and the 2008 earthquake-triggered Wenjiagou (Zhang et al. 2016) rock avalanches, such abrupt slope

breaks exist only at the slope toe, where the sliding rock mass collided with the ground and were fragmented. Even if there were several breaks along the transport path in other rock avalanches, the rock mass would be fragmented only near these abrupt breaks according to the hypothesis, which does not account for the fact that the granular debris in the rock avalanche deposits is consecutively reduced in grain size along the transport path according to Zhang et al. (2016), Perinotto et al. (2015), and this study.

From the above analysis, it seems that only shear-induced fragmentation is a reasonable mechanism for pervasive fragmentation of grains in the rock avalanche during runout. Furthermore, it can adequately explain the grain distribution in the rock avalanche deposit. Shear experiments on riverbed sands conducted by Zhang and McSaveney (2017) indicated that increased normal stress and shear displacement cause more finely fragmented granular grains. This means that average size of grains is reduced from the proximal to the distal end with the increased shear displacement. Meanwhile grains become coarser and coarser from the base up to the surface, as the normal stress at the base is the greatest and gradually diminishes upwards. Moreover, large boulders in the surficial carapace of less than 10 m in thickness are under less confined stress and have free collisions, therefore, are coarser than the underlying debris. Some researchers (Bertran 2003; Imre et al. 2010; Wang et al. 2015) proposed that this inverse grading distribution in the cross section of rock avalanche deposits is formed due to collision and sieving effects. This is obviously contrary to preservation of stratigraphic sequence in the deposit.

Loose soil, especially the saturated loose soil on the transport path entrained and mixed into the granular debris (Dufresne et al. 2010; Wang et al. 2015), has been considered by some scientists to be the most important factor reducing frictional resistance between the bottom of the granular debris and the ground, and therefore, could facilitate the transport of the rock avalanche (Evans et al. 2001; Sassa et al. 2004, 2010; Pudasaini and Miller 2012; Pudasaini 2012; Luna et al. 2012). Dufresne et al. (2010) and Dufresne (2012) conducted a laboratory analogue experiment illustrating the processes of saturated substrate deformation features at the Round Top rock avalanche in New Zealand that indicated how decelerating upper material can be passively transported a further distance on top of a still mobile, low unit. Sassa et al. (2010), Hungr (1995), and Crosta et al. (2009) have also tried to prove the role of saturated substrate in facilitating the runout of rock avalanches using numerical modeling.

Our modeling results, however, indicate that the loose soil on the path surface over which granular debris is transported could not be largely entrained into the bottom of the debris. Instead, it was bulldozed to the front and passively pushed, moving together with the very front part of the rock debris. Some hummocks have formed in the loose soil due to compression by the rock debris. Therefore, from the perspective of energy and momentum balance, the colluvial soil inhabits rather than promotes the long-runout and high speed of the rock avalanche. The hummocks indicate that the colluvial soil has slowed down the rock avalanche debris. This phenomenon was also found at some locations in the Round Top rock avalanche deposit in New Zealand, but was not the general mechanism for the entire rock avalanche (Dufresne et al. 2010). It can be inferred from our findings that colluvial soil on the transport path does not always enhance the transport of rock avalanches.

Conclusions

Field investigation and numerical modeling were conducted to investigate the characteristics of the Jiweishan rock avalanche, and in particular the fragmentation mechanisms of grains during runout. Several conclusions have been reached as follows:

- (1) Deposits of the Jiweishan rock avalanche could be divided into spray, proximal, transport, and distal areas based on their lithological and particle-size distribution. The stratigraphic sequence in the original sliding rock mass is preserved in the deposit, and average grain size decreases from the surface to the bottom, and from the proximal to the distal ends. Large boulders distributed in the surficial carapace were passively carried by the lower finer debris.
- (2) The loose soil on the ground where the rock mass transported was bulldozed to the front rather than incorporated into the bottom of the debris. Therefore, the undrained-loading theory widely used to explain high mobility of rock avalanches does not seem to be applicable to the Jiweishan rock avalanche.
- (3) Under the carapace, the debris moved as a dense granular flow during runout, and shear-induced fragmentation seems to be the only reasonable mechanism for the pervasive fragmentation in the rock avalanche. Furthermore, it could well explain the particle-size distribution in the rock avalanche deposit.>

Acknowledgements

We thank Dr. Eileen McSaveney very much for editing our manuscript and helping to make it more readable.

Funding information This work was supported by the National Natural Science Foundation of China (41472264; 41772334).

References

- Aladejare AE, Wang Y (2017) Evaluation of rock property variability. *Georisk* 11(1):22–41
- Bertran P (2003) The rock-avalanche of February 1995 at Claix (French Alps). *Geomorphology* 54(3):339–346
- Cagnoli B, Manga M (2004) Granular mass flows and Coulomb's friction in shear cell experiments: implications for geophysical flows. *J Geophys Res Solid Earth* 109:F04005
- Cagnoli B, Piersanti A (2017) Combined effects of grain size, flow volume and channel width on geophysical flow mobility: three-dimensional discrete element modeling of dry and dense flows of angular rock fragments. *Solid Earth* 8:177–188
- Cagnoli B, Romano GP (2013) Vertical segregations in flows of angular rock fragments: experimental simulations of the agitation gradient within dense geophysical flows. *J Volcanol Geotherm Res* 265:52–59
- Campbell CS (2006) Granular material flows- an overview. *Powder Technol* 162:208–229
- Chen XY, Zhang LL, Chen LH, Li X, Liu DS (2019) Slope stability analysis based on the Coupled Eulerian-Lagrangian finite element method. *B Eng Geol Environ*. <https://doi.org/10.1007/s10064-018-1413-4>
- Cox SC, McSaveney MJ, Spencer J, Allen SK, Ashraf S, Hancox GT, Sirguey P, Salichon J, Ferris BG (2015) Rock avalanche on 14 July 2014 from Hillary Ridge, Aoraki/ Mount Cook, New Zealand. *Landslides* 12(2):395–402
- Crosta GB, Frattini P, Fusi N (2007) Fragmentation in the Val Pola rock avalanche, Italian Alps. *J Geophys Res* 112:F01006
- Crosta GB, Imposimato S, Roddeman D (2009) Numerical modeling of entrainment/deposition in rock and debris-avalanches. *Eng Geol* 109:135–145
- Davies TRH (1982) Spreading of rock avalanche debris by mechanical fluidization. *Rock Mech* 15:9–24
- Davies TRH, McSaveney MJ (1999) Runout of dry granular avalanches. *Can Geotech J* 36(2):313–320
- Davies TRH, McSaveney MJ (2009) The role of rock fragmentation in the motion of large landslides. *Eng Geol* 109:67–79
- Davies TR, McSaveney MJ (2012) Mobility of long-runout rock avalanches. In: Clague JJ, Stead D (eds) *Landslides – Types, Mechanisms and Modeling*. Cambridge University Press, Cambridge, pp 50–59
- Davies TRH, McSaveney MJ, Hodgson KA (1999) A fragmentation-spreading model for long-runout rock avalanches. *Can Geotech J* 36:1096–1110
- De Blasio FV (2011) Dynamical stress in force chains of granular media traveling on a bumpy terrain and the fragmentation of rock avalanches. *Acta Mech* 221(3–4):375–382
- De Blasio FV, Crosta GB (2014) Simple physical model for the fragmentation of rock avalanches. *Acta Mech* 225:243–252
- De Blasio FV, Crosta GB (2015) Fragmentation and boosting of rock falls and rock avalanches. *Geophys Res Lett* 42(20):8463–8470
- Deparis J, Jongmans D, Cotton F, Baillet L, Thouvenot F, Hantz D (2008) Analysis of rock-fall and rock-fall avalanche seismograms in the French Alps. *Bull Seismol Soc Am* 98(4):1781–1796
- Dufresne A (2012) Granular flow experiments on the interaction with stationary runout path materials and comparison to rock avalanche events. *Earth Surf Process Landf* 37:1527–1541
- Dufresne A, Dunning SA (2017) Process dependence of grain size distributions in rock avalanche deposits. *Landslides* 14:1555–1563
- Dufresne A, Davies TR, McSaveney MJ (2010) Influence of runout-path material on emplacement of the Round Top rock avalanche, New Zealand. *Earth Surf Processes Landforms* 35:190–201
- Dufresne A, Prager C, Bosmeier A (2016) Insights into rock avalanche emplacement processes from detailed morpho-lithological studies of the Tschirgant deposit (Tyrol, Austria). *Earth Surf Process Landf* 41:587–602
- Dunning SA (2004) Rock avalanches in high mountains—a sedimentological approach. PhD thesis, University of Luton, U.K.
- Dunning SA (2006) The grain size distribution of rock-avalanche deposits in valley-confined settings. *Ital J Eng Geol Env* 1:117–121
- Eisbacher GH (1979) Cliff collapse and rock avalanches (sturzstroms) in the Mackenzie Mountains, northwestern Canada. *Can Geotech J* 16:309–334
- Estep J, Dufek J (2013) Discrete element simulations of bed force anomalies due to force chains in dense granular flows. *J Volcanol Geotherm Res* 254:108–117
- Evans SG, Hungr O, John JC (2001) Dynamics of the 1984 rock avalanche and associated distal debris flow on Mount Cayley, British Columbia, Canada, implication for landslide hazard assessment on dissected volcanoes. *Eng Geol* 61:29–51
- Forlati F, Gioda G, Scavia C (2001) Finite element analysis of a deep-seated slope deformation. *Rock Mech Rock Eng* 34(2):135–159
- Friedmann SJ, Taberlet N, Losert W (2006) Rock-avalanche dynamics: insights from granular physics experiments. *Int J Earth Sci* 95(5):911–919
- Hewitt K, Clague JJ, Orwin JF (2008) Legacies of catastrophic rock slope failures in mountain landscapes. *Earth Sci Rev* 87:1–38
- Hungr O (1995) A model for the runout analysis of rapid flow slides, debris flows, and avalanches. *Can Geotech J* 32(4):610–623
- Hutter K, Koch T, Pluuss C, Savage SB (1995) The dynamics of avalanches of granular materials from initiation to runout. Part II. Experiments. *Acta Mech* 109(1–4):127–165
- Imre B, Laue J, Springman SM (2010) Fractal fragmentation of rocks within sturzstroms: insight derived from physical experiments within the ETH geotechnical drum. *Granul Matter* 12:267–285
- Itasca Consulting Group (Itasca) (2004) Particle flow code in 2 dimensions (Version 3.1). Minneapolis, Minnesota, USA
- Legros F (2002) The mobility of long-runout landslides. *Eng Geol* 63:301–331
- Li W, Li H, Dai F, Lee LM (2012) Discrete element modeling of a rainfall-induced flowslide. *Eng Geol* 149–150:22–34
- Lucas A, Mangeney A, Ampuero JP (2014) Frictional velocity-weakening in landslides on Earth and on other planetary bodies. *Nat Commun* 5:3417
- Luna BQ, Remaitre A, van Asch TWJ, Malet JP, van Westen CJ (2012) Analysis of debris flow behavior with a one dimensional run-out model incorporating entrainment. *Eng Geol* 128:63–75
- Manzella I, Labouse V (2008) Qualitative analysis of rock avalanches propagation by means of physical modeling of non-constrained gravel flows. *Rock Mech Rock Eng* 41(1):133–151
- McDougall S, Boulton N, Hungr O, Stead D, Schwab JW (2006) The Zymoetz River landslide, British Columbia, Canada: description and dynamic analysis of a rock slide-debris flow. *Landslides* 3:195–204
- McSaveney MJ, Davies TRH (2009) Surface energy is not one of the energy losses in rock comminution. *Eng Geol* 109:109–113

- Munjiza A (1999) Fracture, fragmentation and rock blasting models in the combined finite-discrete element method. In: Aliabadi MH (ed) *Fracture of rock*. WIT Press, Southampton, pp 125–166
- Nicoletti PG, Sorriso-Valvo M (1991) Geomorphic controls of the shape and mobility of rock avalanches. *Geol Soc Am Bull* 103:1365–1373
- Okura Y, Kitahara H, Sammori T, Kawanami A (2000) The effects of rockfall volume on runout distance. *Eng Geol* 58(2):109–124
- Pedrazzini A, Froese CR, Jaboyedoff M, Hungr O, Humair F (2012) Combining digital elevation model analysis and run-out modeling to characterize hazard posed by a potentially unstable rock slope at Turtle Mountain, Alberta, Canada. *Eng Geol* 128:76–94
- Perinotto H, Schneider J, Bachelery P, Le Bourdonnec F, Famin V, Michon L (2015) The extreme mobility of debris avalanches: a new model of transport mechanism. *J Geophys Res Solid Earth* 120:1–10
- Pirulli M (2009) The Thurwieser rock avalanche (Italian alps): description and dynamic analysis. *Eng Geol* 109(1–2):80–92
- Pirulli M, Preh A, Roth W, Scavia C, Poisel R (2003) Rock avalanche run out prediction: combined application of two numerical methods. ISRM2003-Technology Roadmap for Rock Mechanics. South African Institute of Mining and Metallurgy
- Prager C (2010) *Geologie, Alter und Struktur des Fernpass Bergsturzes und tiefgründiger Massenbewegungen in seiner Umgebung (Tirol, Österreich)*, PhD Thesis. Universität Innsbruck, Austria; 307 p
- Preuth T, Bartelt P, Korup O, McARDell BW (2010) A random kinetic energy model for rock avalanches: eight case studies. *J Geophys Res* 115:F03036
- Pudasaini SP (2012) A general two-phase debris flow model. *J Geophys Res* 117:1–28
- Pudasaini SP, Miller SA (2012) Buoyancy induced mobility in two-phase debris flow. *AIP Conf Proc Am Inst Phys* 1479(1):149–152
- Pudasaini SP, Miller SA (2013) The hypermobility of huge landslides and avalanches. *Eng Geol* 157:124–132
- Quecedo M, Pastor M, Herreros MI, Fernández Merodo JA (2004) Numerical modelling of the propagation of fast landslides using the finite element method. *Int J Numer Methods Eng* 59:755–794
- Richefu V, Mollon G, Daudon D, Villard P (2012) Dissipative contacts and realistic block shapes for modeling rock avalanches. *Eng Geol* 149–150:78–92
- Sassa K, Fukuoaka H, Wang G, Ishikawa N (2004) Undrained dynamic-loading ring shear apparatus and its application to landslide dynamics. *Landslides* 1:7–19
- Sassa K, Nagai O, Solidum R, Yamazaki Y, Ohta H (2010) An integrated model simulating the initiation and motion of earthquake and rain induced rapid landslides and its application to the 2006 Leyte landslide. *Landslides* 7:219–236
- Savage S, Hutter K (1989) The motion of a finite mass of granular material down a rough incline. *J Fluid Mech* 199:177–215
- Savage SB, Hutter K (1991) The dynamics of avalanches of granular materials from initiation to runout. Part I: analysis. *Acta Mech* 86(1–4):201–223
- Scheidegger AE (1973) On the prediction of the reach and velocity of catastrophic landslides. *Rock Mech* 5:231–236
- Shreve RL (1968) The Blackhawk landslides. *Geol Soc Am Spec* 108:47
- Smith GM, Davies TR, McSaveney MJ, Bell DH (2006) The Acheron rock avalanche, Canterbury, New Zealand- morphology and dynamics. *Landslides* 3:62–72
- Sosio R, Crosta GB, Hungr O (2008) Complete dynamic modeling calibration for the Thurwieser rock avalanche (Italia Central Alps). *Eng Geol* 100:11–26
- Staron L (2008) Mobility of long runout rock flows: a discrete numerical investigation. *Geophys J Int* 172(1):455–463
- Staron L, Hinch EJ (2005) Study of the collapse of granular columns using two dimensional discrete-grain simulation. *J Fluid Mech* 545:1–27
- Strom AL (2004) Rock avalanches of the Ardon River valley at the southern foot of the Rocky Rang, Northern Caucasus, North Osetia. *Landslides* 1:237–241
- Taboada A, Chang KJ, Radjai F, Bouchette F (2005) Rheology, force transmission, and shear instabilities in frictional granular media from biaxial numerical tests using the contact dynamics method. *J Geophys Res* 110:B09202
- Taboada A, Estrada N, Radjai F (2006) Additive decomposition of shear strength in cohesive granular media from grain-scale interactions. *Phys Rev Lett* 97:098302
- Tang C, Hu J, Lin M, Angelier J, Lu C, Chan Y, Chu H (2009) The Tsaoling landslide triggered by the Chi-Chi earthquake, Taiwan: insights from a discrete element simulation. *Eng Geol* 106:1–19
- Wang Y, Cheng Q, Zhu Q (2015) Surface microscopic examination of quartz grains from rock avalanche basal facies. *Can Geotech J* 52:167–181
- Wang Y, Xu Q, Cheng Q, Li Y, Luo Z (2016) Spreading and deposit characteristics of a rapid dry granular avalanche across 3D topography: experimental study. *Rock Mech Rock Eng* 49(11):4349–4370
- Weidinger JT, Korup O, Munack H, Altenberger U, Dunning SA, Tippelt G, Lottermoser W (2014) Giant rockslide from the inside. *Earth Planet Sci Lett* 389:62–73
- Wu LZ, Zhou Y, Sun P, Shi JS, Liu GG, Bai LY (2017) Laboratory characterization of rainfall-induced loess slope failure. *CATENA* 150:1–8
- Wu LZ, Deng H, Huang RQ, Zhang LM, Guo XG, Zhou Y (2019) Evolution of lakes created by landslide dams and the role of dam erosion: a case study of the Jiajun landslide on the Dadu River, China. *Quatern Int.* <https://doi.org/10.1016/j.quaint.2018.08.001>
- Xing a, Wang G, Yin Y, Jiang Y, Wang G, Yang S, Dai D, Zhu Y, Dai J (2014) Dynamics analysis and field investigation of a fluidized landslide in Guanling, Guizhou, China. *Eng Geol* 181:1–14
- Xu Q, Fan X, Huang R, Yin Y, Hou S, Dong X, Tang M (2010) A catastrophic rockslide-debris flow in Wulong, Chongqing, China in 2009: background, characterization, and causes. *Landslides* 7:75–87
- Yin Y, Wang F, Sun P (2009) Landslide hazards triggered by the 2008 Wenchuan earthquake, Sichuan, China. *Landslides* 6(2):139–152
- Yin Y, Sun P, Zhu J, Yang S (2011a) Research on catastrophic rock avalanche at Guanling, Guizhou, China. *Landslides* 8(4):517–525
- Yin Y, Sun P, Zhang M, Li B (2011b) Mechanism on apparent dip sliding of oblique inclined bedding rockslide at Jiweishan, Chongqing, China. *Landslides* 8(1):49–65
- Yin Y, Wang W, Zhang N, Yan J, Wei Y (2017) The June 2017 Maoxian landslide: geological disaster in an earthquake area after the Wenchuan Ms 8.0 earthquake. *Sci China Technol Sci* 60(11):1–5
- Zhang J (2015) Transport dynamics of the Jiweishan rock avalanche in Wulong County, Chongqing, China. Master Thesis, China University of Geosciences, China, 71p
- Zhang M, McSaveney M (2017) Rock avalanche deposits store quantitative evidence on internal shear during runout. *Geophys Res Lett* 44:8814–8821
- Zhang M, McSaveney M (2018) Is air pollution causing landslides in China? *Earth Planet Sci Lett* 481:284–289
- Zhang M, Yin Y (2013) Dynamics, mobility-controlling factors and transport mechanisms of rapid long-runout rock avalanches in China. *Eng Geol* 167:37–58
- Zhang M, Yin Y, Wu S, Zhang Y, Han J (2011) Dynamics of the Niumiangou Creek rock avalanche triggered by 2008 M_s 8.0 Wenchuan earthquake, Sichuan, China. *Landslides* 8(3):363–371
- Zhang M, Yin Y, McSaveney MJ (2016) Dynamics of the 2008 earthquake-triggered Wenjiagou Creek rock avalanche, Qingping, Sichuan, China. *Eng Geol* 200:75–87
- Zhang M, McSaveney M, Shao H, Zhang C (2018) The 2009 Jiweishan rock avalanche, Wulong, China: precursor conditions and factors leading to failure. *Eng Geol* 233:225–230

M. Zhang

Faculty of Engineering,
China University of Geosciences,
388#, Lumo Road, Wuhan, Hubei Province 430074, People's Republic of China

L. Wu

State Key Laboratory of Geohazard Prevention and Geoenvironment Protection,
Chengdu University of Technology,
Chengdu, Sichuan Province 610059, People's Republic of China
Email: wulizhou07@cudt.cn

J. Zhang

Qinghai Institute of Geo-Environment Monitoring,
Xining, Qinghai Province 810008, People's Republic of China

L. Li

Department of Geology and Geological Engineering,
South Dakota School of Mines and Technology,
501 E. Saint Joseph St., Rapid City, SD 57701, USA